Green's-function approach to atomic many-body calculations with application to the ground state in alkali-metal atoms

Håkan Warston, Ingvar Lindgren, and Sten Salomonson
Department of Physics, Chalmers University of Technology and Göteborg University, S-412 96 Göteborg, Sweden
(Received 27 November 1996)

In this paper we apply the single-particle Green's-function method to the atomic many-body perturbation theory. We present an all-order evaluation scheme for the proper self-energy operator based on the systematic use of Dyson's integral equations. The method is complete to third order in perturbation theory and, in addition, large classes of higher-order effects are included by solving the Dyson equations. Certain classes of many-body correlation effects beyond the pair-correlation approximation are included. The proposed method is tested by calculating the ground-state valence-electron binding energy for the alkali-metal atoms Li, Na, and K. Agreement with experimental results corresponds to an error in the correlation energy contribution of 3–4 %. If certain three-particle effects, not evaluated in this work, are added, the agreement with experiments is, for sodium and potassium, approximately within 1% of the correlation energy. [S1050-2947(97)08604-6]

PACS number(s): 31.10.+z, 31.15.Ar, 31.15.Md, 31.25.Eb

I. INTRODUCTION

During the last decades, several methods have been developed for performing accurate atomic and molecular structure calculations. In particular, the multiconfiguration Hartree-Fock method and the many-body perturbation theory (MBPT) have been used successfully to evaluate atomic properties, e.g., binding energies and hyperfine structures. The MBPT approach based on the works by Brueckner and Goldstone was first applied by Kelly to closed-shell atoms and other atomic systems being described with a single-determinant wave function [1–4]. The approach was later generalized to open-shell systems by Brandow, Sandars, and Lindgren [5, 6, and 7, respectively]. A comprehensive treatment of atomic MBPT can be found in Ref. [8]. Perturbative procedures, however, become unmanageable beyond third order due to the exploding number of terms in the perturbation series. This has led to the development of various non-perturbative schemes of which the coupled-cluster (CC) method, first developed by Coester and Kümmel [9,10] in nuclear physics and then introduced into quantum chemistry by Čížek [11,12], is so far the most powerful and widely used procedure. The CC method has been successfully applied to atomic-structure calculations in the coupled-cluster singles and doubles (CCSD) approximation, where only the one-electron and two-electron correlation effects are retained [8,13–15].

In the coupled-cluster approach, however, it has turned out to be difficult to go beyond the pair-correlation approximation and include correlation between more than two electrons in a systematic way. There are small but significant discrepancies between the experimentally measured binding energies and the ones calculated using the CCSD method. It is reasonable to assume that these discrepancies are largely due to many-body correlation effects beyond the pair-correlation approximation. Even for alkali atoms, with a single electron outside a closed core, these many-body correlation effects make significant contributions to the binding energy. For the binding energy of the $3s$ electron in sodium, only 94% of the correlation energy can be explained as pair correlation. For $4s$ in potassium, the CCSD result for the binding energy agrees well with experiment. This agreement, however, seems fortuitous, since certain classes of effects beyond the CCSD approximation have been evaluated by Ynnerman [16] and found to decrease the correlation energy with 6.5%. The correlation energy is therefore also underestimated in potassium. It is therefore of interest to find methods where classes of many-body effects beyond the pair-correlation approximation can be included systematically to all orders in perturbation theory.

In this paper we apply an alternative approach to the atomic many-body theory, the single-particle Green's-function method, which is based on the time-dependent formulation of perturbation theory and the diagrammatic formulation of quantum field theory by Feynman, Gell-Mann, Dyson, and others [17–21]. The method is formulated in terms of renormalized or dressed electron propagators and screened Coulomb interaction lines. The ideas behind the renormalization (inclusion of electron-correlation effects to infinite order in perturbation theory) of the electron propagator and the Coulomb interaction for many-body systems are well known and have been used frequently in solid-state physics. See, for example, the textbooks by Fetter and Walecka [22] and by Mattuck [23]. The electron correlation is described, in this approach, by the so-called *self-energy operator*. In this method, correlation effects are included to higher orders in a straightforward manner by evaluating the effect to lowest order and then solving the appropriate Dyson equation for the effect.

There are several advantages with such a formulation of the atomic many-body theory. First of all, a formulation in terms of non-time-ordered Feynman diagrams is much more compact than the ordinary diagrammatic formulation of MBPT in terms of time-ordered Goldstone diagrams. Second, all possible time orders of the interaction lines are automatically included in the evaluation of the Feynman diagram. This is not the case, for example, in the CCSD, where time orders describing three-electron correlation effects are

omitted and other time orders need to be explicitly included in order to include Hermitian conjugates of certain classes of effects. A third advantage is that the approach is Hermitian, in contrast to, e.g., the coupled-cluster approach in intermediate normalization [24].

Single-particle Green's-function methods have been used extensively in quantum chemistry to calculate binding energies and electron affinities for molecules. Reviews on how the Green's-function methods are applied in quantum chemistry are given by Linderberg and Ohrn [25,26], by Cederbaum and Domcke [27], by von Niessen, Schirmer, and Cederbaum [28], and also by Oddershede [29]. Many of the reported calculations in quantum chemistry where single-electron Green's-function methods are used are, however, performed in the so-called *two-particle one-hole Tamm-Dancoff approximation* (2ph TDA), where the leading contributions to the ground-state correlation are only partly accounted for, yielding a relatively poor agreement between the calculated binding energies and the experimental results. In the *extended 2ph TDA* method [30], which is complete to third order in perturbation theory, the leading contributions to the ground-state correlation are included and the agreement between theory and experiment is significantly improved.

In 1983, Schirmer, Cederbaum, and Walter [31] introduced the *Algebraic Diagrammatic Construction* (ADC) method, which can be used to devise systematic approximations for the Green's function. In the ADC approach the diagrammatic expansion of the proper self-energy operator is combined with an assumed algebraic form for the proper self-energy operator. The algebraic equation is expanded in a perturbation series and the terms in the series are then identified with the diagrams of the same order in the diagrammatic expansion. In this way, approximations of the functions included in the algebraic equation can be generated. The approximations are then substituted back into the original equation and the self-energy operator is calculated. The self-energy operator calculated in this way includes infinite partial summations of contributions. With this approach, systematic approximations can be devised by identifying the diagrams in the expansion to a certain order in perturbation theory. The ADC approach including all third-order effects, ADC(3), was shown to yield the same results as the extended 2ph TDA approximation. A drawback of the ADC method, however, seems to be that the identification of the higher-order contributions, included in the self-energy beyond the diagrams used when devising the approximation, is nontrivial. The infinite class of correlation effects included in the proper self-energy operator is therefore hard to identify.

The method of including electron correlation by evaluating the proper self-energy operator has also been used when treating different types of scattering processes on atoms. Amusia and Cherepkov have used the *random-phase-approximation-with-exchange* (RPAE) method in their calculations of photoionization cross sections and inelastic scattering of electrons on atoms [32]. Also Wendin and Ohno [33,34] and others have used similar RPAE methods when investigating correlation effects for core holes induced in heavy atoms. A thorough discussion of both theoretical and experimental aspects of the photoionization process is given in the review paper by Wendin [35].

The Green's-function method has also been used in atomic MBPT calculations by Dzuba *et al.* [36–39] in their calculations of the properties of cesium and negative alkali ions. In these works they have, however, focused on the effect of screening of the Coulomb interaction and only included a subset of the leading correlation contributions to all orders. The importance of a systematic inclusion of all low-order correlation contributions was demonstrated by Blundell, Johnson, and Sapirstein [40] in their calculations of the ground-state energies of cesium and thallium. In the present work, correlation effects are included systematically to all orders in perturbation theory. All effects that appear in second and third order and also a large fraction of those appearing in fourth order are included in the proper self-energy operator. Furthermore, large classes of higher-order effects are included by solving the Dyson equations.

It is the purpose of the present paper to test our procedure on the alkali atoms lithium, sodium, and potassium, which all have a single valence electron outside a closed core. The correlation energies and binding energies for the ground state are compared with other calculations as well as with experimental data.

The plan of this paper is the following. In Sec. II a brief review of the theoretical methods on which our work is based is given. Special attention is given to the proper self-energy operator and the proper polarization operator, which are fundamental cornerstones in the method. In Sec. III a schematic overview of the numerical procedure and the results are given. The results are discussed and special attention is given to the difference between the inclusion of only the low-order contributions and a systematic inclusion of the effects to all orders using Dyson equations. The method is compared with similar results from calculations using the CCSD approach. A short summary and some conclusions are given in Sec. IV.

II. THEORY

The formalism on which our computational procedure is based has been described in detail in the literature [8,22,23], but for the convenience of the reader a summary is given here as a basis for the following treatment. We are using atomic units where $e=m=\hbar=4\pi\varepsilon_0=1$.

A. Basic formalism

We consider a N-electron atomic system with a nondegenerate ground state $|\Psi^0\rangle$. The nonrelativistic atomic Hamiltonian describing this system,

$$\hat{H}=-\frac{1}{2}\sum_{n=1}^{N}\nabla_n^2-\sum_{n=1}^{N}\frac{Z}{r_n}+\sum_{m<n}^{N}\frac{1}{r_{mn}}, \tag{1}$$

is partitioned into an unperturbed Hamiltonian,

$$\hat{H}_0=\sum_{n=1}^{N}\left(-\frac{1}{2}\nabla_n^2-\frac{Z}{r_n}+U(\mathbf{r}_n)\right)=\sum_{n=1}^{N}\hat{h}_0(\mathbf{r}_n) \tag{2}$$

and a perturbation

$$\hat{H}_1=\hat{H}-\hat{H}_0=\sum_{m<n}^{N}\frac{1}{r_{mn}}-\sum_{n=1}^{N}U(\mathbf{r}_n). \tag{3}$$

The model potential can be written as

$$U(\mathbf{r_2})\varphi=\int d^3r_1[u_l(\mathbf{r}_2,\mathbf{r}_1)+u_{nl}(\mathbf{r}_2,\mathbf{r}_1)]\varphi(\mathbf{r}_1). \tag{4}$$

At this stage no assumptions are made about the model potential. It is considered to be a general model potential containing both local (l) and nonlocal (nl) parts, where the former is given by

$$u_l(\mathbf{r}_2,\mathbf{r}_1)=\delta(\mathbf{r}_2-\mathbf{r}_1)U_l(\mathbf{r}_2). \tag{5}$$

The single-particle equation

$$\hat{h}_0|\varphi_i\rangle=\varepsilon_i|\varphi_i\rangle \tag{6}$$

defines a set of electron orbitals, which form the basis of the calculation. The Slater determinants $|\Phi^A\rangle$ formed by these orbitals are antisymmetrized eigenfunctions of $\hat{H}_0$,

$$\hat{H}_0|\Phi^A\rangle=E_0^A|\Phi^A\rangle \tag{7}$$

with the eigenvalue equal to the sum of the orbital eigenvalues of the determinant

$$E_0^A=\sum_{i}^{occ}\varepsilon_i. \tag{8}$$

We are considering alkali atoms, which have a single electron outside a closed core. Such systems can be treated in MBPT as effective one-body systems. The propagation of the outer electron between two points $\mathbf{r}t$ and $\mathbf{r}'t'$ in space-time, while interacting with the nucleus and all the electrons in the core, is described by the *exact* single-particle Green's function $G(\mathbf{r}'t',\mathbf{r}t)$, also known as the *electron propagator*. Evaluation of the exact electron propagator is of the same degree of complexity as solving the full Schrödinger equation for the atom. From the formal definition, which can be found in the literature (see, for example, Refs. [22,23]), it is possible to show that the exact propagator can be written in the interaction picture as a perturbation expansion as

$$\begin{aligned}iG(\mathbf{r}'t',\mathbf{r}t)=\sum_{m=0}^{\infty}\frac{(-i)^m}{m!}\int_{-\infty}^{\infty}dt_1\ldots\int_{-\infty}^{\infty}dt_m\\ \times\langle\Phi^0|T[\hat{H}_1(t_1)\ldots\hat{H}_1(t_m)\\ \times\hat{\psi}(\mathbf{r}'t')\hat{\psi}^\dagger(\mathbf{r}t)]|\Phi^0\rangle_{connected}.\end{aligned} \tag{9}$$

Here, $|\Phi^0\rangle$ is the ground state for the unperturbed system described by $\hat{H}_0$. $T[\cdots]$ denotes a time-ordered product that implies that the operators should be reordered from right to left with increasing time. $\hat{H}_1(t)$ is the perturbation in second-quantized form for a single electron, i.e., the difference between the Coulomb interaction with the electrons in the core and the model potential $u(\mathbf{r}_2,\mathbf{r}_1)$. $\hat{\psi}(\mathbf{r}'t')$ and $\hat{\psi}^\dagger(\mathbf{r}t)$ are the field operators in second quantization, given by

$$\begin{aligned}\hat{\psi}(\mathbf{r}'t')&=\sum_k\varphi_k(\mathbf{r}')e^{-i\varepsilon_kt'}\hat{a}_k,\\ \hat{\psi}^\dagger(\mathbf{r}t)&=\sum_k\varphi_k^\star(\mathbf{r})e^{i\varepsilon_kt}\hat{a}_k^\dagger,\end{aligned} \tag{10}$$

where the $\varphi_k(\mathbf{r})$ are the one-electron eigenfunctions to $\hat{h}_0$ and ε_k the corresponding energy eigenvalues. The summation runs over the complete set of one-particle states. The subscript *connected* in Eq. (9) means that only connected terms contribute, i.e., terms that do not factorize into several independent parts. Equation (9) is analogous to the *linked-diagram theorem* in MBPT, and was first proved by Goldstone [2] to all orders in perturbation theory. The perturbation expansion of the exact electron propagator in Eq. (9) forms the basis for the MBPT formalism employed in this work.

The perturbation $\hat{H}_1(t)$ in second quantized form is given by

$$\begin{aligned}\hat{H}_1(t_1)=\frac{1}{2}\int\int d^3r_1d^3r_2\int dt_2\left\{\hat{\psi}^\dagger(\mathbf{r}_1t_1)\hat{\psi}^\dagger(\mathbf{r}_2t_2)\frac{\delta(t_2-t_1)}{r_{21}}\hat{\psi}(\mathbf{r}_2t_2)\hat{\psi}(\mathbf{r}_1t_1)\right\}\\ -\int\int d^3r_1d^3r_2\int dt_2\{\hat{\psi}^\dagger(\mathbf{r}_2t_2)u(\mathbf{r}_2,\mathbf{r}_1)\delta(t_2-t_1)\hat{\psi}(\mathbf{r}_1t_1)\},\end{aligned} \tag{11}$$

where the first term is the instantaneous Coulomb interaction between two electrons in the field and the second term is the interaction with the model potential. Due to the complex structure of $\hat{H}_1$, even the lowest-order terms in Eq. (9) will have a very complicated form. Wick's theorem [41], however, provides a powerful tool for singling out the contributing terms in the expansion. The theorem states that a time-ordered product of n operators can be written as the normal-ordered product plus the sum of all possible contractions within the normal-ordered product, i.e.,

$$\begin{aligned}T[\hat{A}\hat{B}\hat{C}\cdots\hat{U}]=N[\hat{A}\hat{B}\cdots\hat{U}]+N[\underline{\hat{A}\hat{B}}\hat{C}\cdots\hat{U}]\\ +N[\hat{A}\underline{\hat{B}\hat{C}}\cdots\hat{U}]+\cdots\\ +N[\underline{\hat{A}\hat{B}}\ \underline{\hat{C}\hat{D}}\cdots\hat{U}]+\cdots,\end{aligned} \tag{12}$$

where $\hat{A}\hat{B}$ denotes that the operators are contracted. In Eq. (9) the electron propagator is given as the unperturbed ground-state average $\langle\Phi^0|\cdots|\Phi^0\rangle$. If the time-ordered products in Eq. (9) are expanded using Wicks theorem, only terms that are fully contracted will yield nonzero contributions since the ground-state average of a normal-ordered operator product is zero by definition. Furthermore, the only contractions that are not zero are contractions between $\hat{\psi}$ and $\hat{\psi}^\dagger$. Applying this to the first term in Eq. (9), $m=0$, the zeroth-order electron propagator $G_0(\mathbf{r}'t',\mathbf{r}t)$ can be directly identified as the contraction

$$iG_0(\mathbf{r}'t',\mathbf{r}t)=\underline{\hat{\psi}(\mathbf{r}'t')\hat{\psi}^\dagger(\mathbf{r}t)}. \tag{13}$$

This means that the perturbation expansion of the exact electron propagator in Eq. (9) can be expressed more simply in terms of the zeroth-order electron propagator G_0, the instantaneous Coulomb interaction $1/r_{21}$, and the interaction with the model potential $-u(\mathbf{r}_2,\mathbf{r}_1)$.

If the electron propagator is Fourier transformed with respect to $t-t'$, it is possible to reformulate the expansion of G in a very compact form as

$$G(\mathbf{r}',\mathbf{r},\omega)=G_0(\mathbf{r}',\mathbf{r},\omega)+\int\int d^3r_2d^3r_1G_0(\mathbf{r}',\mathbf{r}_2,\omega)\times\Sigma^\star(\mathbf{r}_2,\mathbf{r}_1,\omega)G(\mathbf{r}_1,\mathbf{r},\omega). \tag{14}$$

The Fourier-transformed zeroth-order electron propagator $G_0(\mathbf{r}',\mathbf{r},\omega)$ is given by

$$G_0(\mathbf{r}',\mathbf{r},\omega)=\sum_m\frac{\varphi_m(\mathbf{r}')\varphi_m^\star(\mathbf{r})}{(\omega-\varepsilon_m+i\eta_m)}\begin{cases}\eta_m<0 & \text{core states}\\ \eta_m>0 & \text{virtual states.}\end{cases} \tag{15}$$

η_m is a small real number added when defining the Fourier transformation to ensure the convergence of the Fourier integrals, and the limit $\eta\to0$ should be taken after the calculation is done. $\Sigma^\star(\mathbf{r}_2,\mathbf{r}_1,\omega)$ in Eq. (14) is the *proper self-energy operator* accounting for the correlation effects beyond the independent-particle model, described by $\hat{H}_0$. Equation (14) is known as the *Dyson equation* for the electron propagator and plays a central role in our treatment. >From the Dyson equation it can be shown that the motion of the outer electron in the presence of the closed-shell system can be described by a *quasiparticle* wave function $\phi(\mathbf{r})$ satisfying the quasiparticle equation (QPE)

$$\hat{h}_0\phi(\mathbf{r})+\int\Sigma^\star(\mathbf{r},\mathbf{r}_1,\varepsilon)\phi(\mathbf{r}_1)d^3r_1=\varepsilon\phi(\mathbf{r}). \tag{16}$$

$\phi(\mathbf{r})$ describes the wave function for the electron *in the presence of the other electrons in the atom*. The effects due to the relaxation of the core electrons in the atom are taken into account in this wave function and $\phi(\mathbf{r})$ is therefore usually referred to as a *quasiparticle orbital*. Having calculated the proper self-energy operator $\Sigma^\star(\varepsilon)$ to some level of approximation, it is added to $\hat{h}_0$ and the QPE is solved in the same way as the zeroth-order equation. Since $\Sigma^\star(\varepsilon)$ is energy dependent, the equation has to be solved self-consistently with respect to ε. The resulting energy eigenvalue is equal to the binding energy of the outer electron.

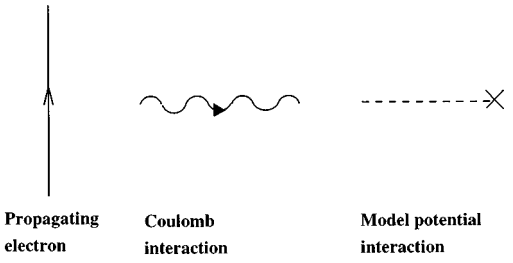

FIG. 1. Graphical representation of the Feynman diagram building blocks.

B. Graphical representation

A graphical representation of the exact electron propagator in Eq. (14) can now be formulated, using the zeroth-order electron propagator G_0, the instantaneous Coulomb interaction $1/r_{21}$, and the interaction with the model potential $-u(\mathbf{r}_2,\mathbf{r}_1)$ as building blocks. In diagrammatic form, the zeroth-order electron propagator is represented by a vertical line; see Fig. 1. The Coulomb interaction is represented by a wavy line and the interaction with the model potential by a dotted line with a cross. The contributions to order n in Eq. (9) can then be constructed in the following way.

(i) Draw all topologically distinct connected diagrams containing n interaction lines and $2n+1$ electron propagator lines.

(ii) The contribution to the electron propagator from each diagram can be constructed following the rules given in Fig. 2.

The diagrammatic expansion of the electron propagator is given to first order in Fig. 3. If the Hartree-Fock (HF) potential from the closed-shell core is used as the zeroth-order model $\hat{h}_0$, the sum of the three first order modifications in Fig. 3 is zero. The use of the HF model substantially reduces

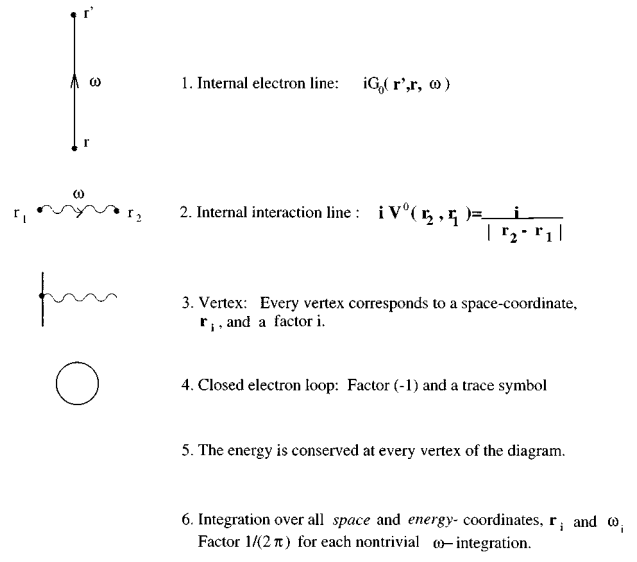

FIG. 2. Rules for evaluating the Feynman amplitudes from a diagram.

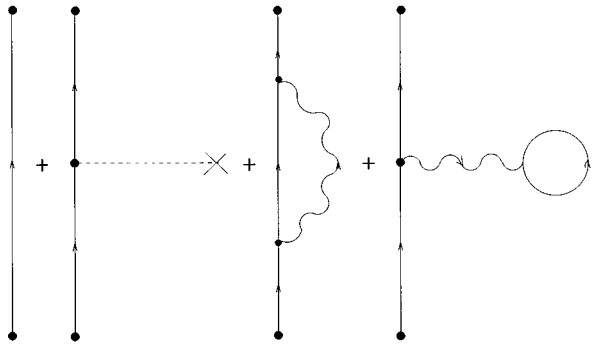

FIG. 3. Graphical representation of the electron propagator to first order in perturbation theory.

the number of contributions to the electron propagator, since all higher-order iterations of the sum of the first-order contributions also yield zero contributions. The first nonvanishing contributions, beyond zeroth order, to the electron propagator, using the HF approximation, are given by the two second-order diagrams in Fig. 4.

The exact electron propagator consists of the unperturbed zeroth-order electron propagator G_0 plus all connected diagrams with a zeroth-order electron propagator at each end. This defines the self-energy operator Σ diagrammatically as a structure which is connected to the rest of the diagram with only two zeroth-order electron lines. It is the self-energy operator that contains all the effects of the perturbation $\hat{H}_1$. The *proper self-energy operator* $\Sigma^\star$ is defined as a structure that *cannot* be divided into two lower-order self-energy operators by cutting a single electron line. The self-energy operator Σ is then given by the proper self-energy operator $\Sigma^\star$ plus the sum of all successive iterations of $\Sigma^\star$,

$$\Sigma=\Sigma^\star+\Sigma^\star G_0\Sigma^\star+\Sigma^\star G_0\Sigma^\star G_0\Sigma^\star+\ldots. \tag{17}$$

The diagrammatic expansion of the electron propagator G in terms of the proper self-energy operator is given in Fig. 5, which is the graphical equivalent of the Dyson equation (14) in the preceding section. An all-order approximation of the electron propagator $G(\mathbf{r}',\mathbf{r},\omega)$ can therefore be calculated by evaluating the proper self-energy operator to some level of approximation and then solving the Dyson equation. This is referred to as *renormalizing* or *dressing* the electron propagator.

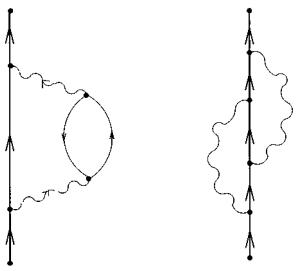

FIG. 4. Second-order contributions to the electron propagator. If using HF as the zeroth-order model, these are the first nonvanishing contributions beyond the zeroth-order approximation G_0.

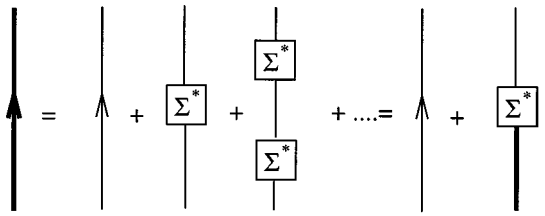

FIG. 5. The diagrammatic formulation of the Dyson equation for the electron propagator $G(\mathbf{r}',\mathbf{r},\omega)$.

Correlation also affects the interaction between the electrons. This is described as screening of the Coulomb interaction. It is taken into account by evaluating the *proper polarization operator* $\Pi^\star(\mathbf{r}_2,\mathbf{r}_1,\omega)\equiv\Pi^\star_{21}(\omega)$. In analogy to the definition of the self-energy operator, the polarization operator Π is defined as a structure connected to the rest of the diagram with only two Coulomb interactions. The *proper polarization operator* $\Pi^\star$ is defined as a structure that *cannot* be divided into two lower-order polarization operators by cutting a single interaction line. The polarization operator Π is given by the proper polarization operator $\Pi^\star$ plus the sum of all successive iterations of $\Pi^\star$,

$$\Pi=\Pi^\star+\Pi^\star V^0\Pi^\star+\Pi^\star V^0\Pi^\star V^0\Pi^\star+\ldots, \tag{18}$$

where in our case $V^0=1/r_{ij}$. The proper polarization of the Coulomb interaction is therefore taken into account to all orders by solving the Dyson equation

$$V_{21}(\omega)=V^0_{21}+\int\int d^3r_3 d^3r_4 V^0_{24}\Pi^\star_{43}(\omega)V_{31}(\omega). \tag{19}$$

Equation (19) is given in diagrammatic form in Fig. 6. An all-order approximation of the screened Coulomb interaction $V_{ij}(\omega)$ can therefore be calculated by evaluating the proper polarization to some level of approximation and then solving the Dyson equation (19).

The proper self-energy operator can be formulated in terms of so-called *skeleton diagrams*. These are obtained by taking a proper self-energy operator and removing all electron self-energy insertions and all polarization insertions on the interaction lines. The remainder is defined as a skeleton diagram for the proper self-energy operator. The same can be done for the proper polarization operator resulting in a set of polarization skeletons. In Fig. 7 the self-energy operator skeletons including up to three interactions are given and in Fig. 8 the skeletons for the polarization including up to two interactions is given. The dressed electron propagators and the screened Coulomb interactions are evaluated from Eqs. (14) and (19) and are then used to calculate the proper self-energy operator and the proper polarization operator from these skeletons in Figs. 7 and 8. A large number of high-order correlation effects are included automatically, using a very limited number of skeleton diagrams. Which skeletons should be included depends on which diagrammatic building blocks are used. In this work we are using the dressed electron propagators and the screened interaction lines as building blocks. If so-called vertex corrections $\Gamma(r_1,r_2,r_3,\omega_1,\omega_2)$ modifying the vertices were also used, then the entire perturbation expansion could be very com-

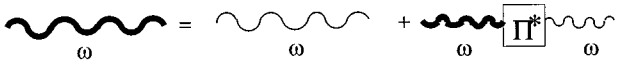

FIG. 6. The diagrammatic formulation of the Dyson equation for the screened Coulomb interaction $V_{ij}(\omega)$.

pactly formulated in terms of only the two first skeletons, 1 and 2, in Fig. 7 and skeleton 1 in Fig. 8. This is, however, not possible today with the computing power we have available, since a general evaluation procedure for vertex corrections would require a very large internal computer memory. For that reason, vertex modifications lead, in our procedure, to distinct skeletons, as illustrated in Figs. 7 and 8.

Finally, the all-order proper self-energy operator is used in the quasiparticle equation (16). The binding-energy of the outer electron is then given by the energy eigenvalue of the quasiparticle equation.

III. NUMERICAL PROCEDURE AND RESULTS

A. Numerical procedure

By the use of dressed electron propagators and screened Coulomb interactions, when evaluating the proper self-energy operator, a considerable amount of higher-order effects are automatically included in the procedure. A general calculation procedure including all self-energy and polarization effects given by Figs. 7 and 8 is, however, not possible with the computational power available today. By the use of certain approximations, a large subset of effects in the theoretical procedure above can be included, though. In this section our computational procedure and the approximations used will be discussed.

As the zeroth-order model of the single-electron Hamiltonian $\hat{h}_0$ we have used the spherically symmetric Hartree-Fock model of the closed-shell positive alkali ion to define the zeroth-order approximation. This means that all electrons in the atom feel the direct and exchange interactions with the electrons described by the HF orbitals from the positive ion. This model is commonly known as the HF V^{N-1} model. The basis functions used in our calculations are obtained using the numerical finite basis set method as described in Ref.

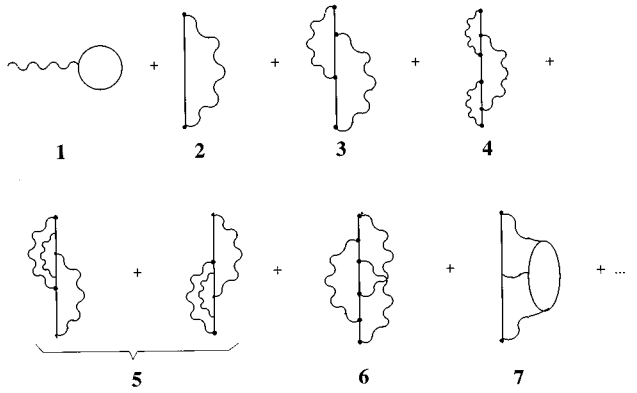

FIG. 7. Graphical expansion of the proper self-energy operator in terms of skeletons. The all-order proper self-energy operator is evaluated from these skeletons using dressed propagators and screened interaction lines.

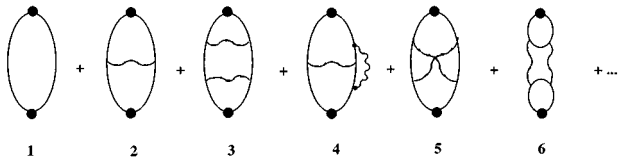

FIG. 8. Graphical expansion of the proper polarization operator in terms of skeletons.

[42]. Since a spherically symmetric model potential is used, only the radial electron propagator $G(r',r,\omega)$, the radial self-energy operator $\Sigma(r_2,r_1,\omega)$, and the radial polarization $\Pi(r_2,r_1,\omega_1)$ need to be evaluated for each angular-momentum symmetry. The angular momentum integrals are handled using the graphical techniques developed in ordinary MBPT; see, for example, Ref. [8].

As pointed out in the preceding section, by using the HF model, the number of diagrams contributing to the self-energy operator is significantly reduced. The first nonvanishing contributions beyond zeroth order are given by the two self-energies in Fig. 4. In third order there are 14 contributing diagrams. Of this number only 12 need to be explicitly calculated, as the remaining two are Hermitian conjugates of two other graphs. In fourth order we have found 122 contributing Feynman diagrams, Hermitian conjugates included, and 34 of these have been evaluated in this work.

When evaluating the dressed electron propagators using the Dyson equation, Eq. (14), we have chosen to truncate the self-energy operator skeletons at the two-interaction-line level; see Fig. 9. The effects included in S_1 in Fig. 9 originate from skeleton 1 in Fig. 7. The leading-order diagram from this skeleton is included in the HF potential and describes how the electron interacts with the average charge density of the core electrons in the system. This diagram is responsible for the main part of the screening of the interaction with the nucleus and the contribution to the binding energy from this diagram is almost as large as the contribution from the interaction with the nucleus, but with opposite sign. The correlation effects given by S_1 in Fig. 9 describe modifications of the average charge density due to correlation effects in the core. Since the first-order contribution to skeleton 1 is so large, it is reasonable to expect that for valence electrons penetrating the core modifications of the skeleton also yields significant contributions to the self-energy operator.

The correlation effects given by S_2 in Fig. 9 describe the attraction between the electron and the core due to the polarization of the core. The core polarization yields by far the most important correlation contributions to the self-energy operator, as will be seen in the results presented later.

Skeletons 3, 4, 5, 6, and 7 in Fig. 7 all describe complicated correlation effects. Skeleton 3 contains only two interaction lines while the others contain three interaction lines. It is reasonable to assume that skeleton 3 yields significantly larger contributions than the other skeletons. Skeleton 3 is therefore included, while skeletons 4, 5, 6, and 7 are neglected, in the self-energy operator which is used for evaluating dressed electron propagators.

For the proper polarization operator $\Pi^{\star}_{21}(\omega_1)$, skeletons 1, 2, and 3 in Fig. 8 have been included, using zeroth-order

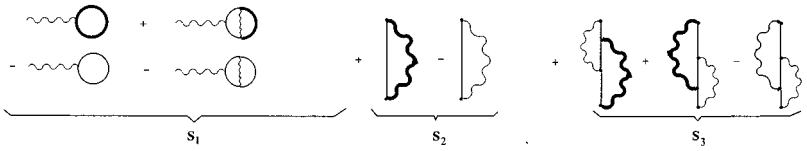

FIG. 9. Graphical representation of the proper self-energy operator $\Sigma(r',r,\omega)$ used for evaluating the dressed electron propagator. The thick lines are dressed using the Dyson equation.

electron propagators and the ordinary Coulomb interaction. The polarization can, in this approximation, be evaluated as a function of the energy ω_1, using ordinary calculus of residues. If modified propagators and interaction lines are included in the polarization, numerical integration methods have to be used for the energy integrations included in the polarization. This is far more demanding computationally and is not done in this work.

For the proper self-energy operator $\Sigma^\star(\varepsilon)$, used when solving the quasiparticle Eq. (16), a larger set of skeletons is included than for the self-energy operator used for dressing the electron propagator. The most computationally demanding diagrammatic structures in our approach are the so-called vertex corrections $\Gamma(r_1,r_2,r_3,\omega_1,\omega_2)$; see Fig. 10. The ability to evaluate the different contributions to the vertex correction will limit how many of the skeletons in Figs. 7 and 8 can be included. In this work we have used the approximation given in Fig. 11 for the vertex corrections, when modifying the vertices in skeleton 2 in Fig. 7. In this way, skeletons 3, 4, and 5 in Fig. 7 are generated. This approximation for the vertex correction will lead to the self-energy operator given in Fig. 12, used when solving the quasiparticle Eq. (16). In this approximation skeletons 6 and 7 in Fig. 7 are not included. In order to make the self-energy operator complete to third order in perturbation theory, however, the lowest-order contributions to the skeletons, depicted in Fig. 13 have been added to the self-energy operator.

The numerical procedure employed in this work is schematically divided into five different steps.

(1) A proper polarization operator $\Pi^\star(r_2,r_1,\omega_1)$ is first evaluated in the approximation given above. The evaluated polarization is used when setting up the Dyson equation (19) for the screened interaction $V_{ij}(\omega_1)$. In this way a set of screened interaction lines is generated.

(2) A proper self-energy operator $\Sigma^\star(r_2,r_1,\omega)$, which should be used for evaluating the dressed electron propagators, is calculated. The calculation of $\Sigma^\star(r_2,r_1,\omega)$ is performed in two steps. In the first step, the self-energy contributions from S_2 and S_3 in Fig. 9 are calculated using zeroth-order propagators and screened interaction lines, evaluated from the Dyson equation (19) with the approximation for the polarization discussed above. S_2 and S_3 are used together with the Dyson equation (14) in order to calculate a first set of dressed electron propagators. In the second step, these propagators are used in the evaluation of the self-energy operator S_1 in Fig. 9. S_1 is then added to S_2+S_3. The proper self-energy operator in Fig. 9 can be written as

$$
\begin{aligned}
i\Sigma^\star(r_2,r_1,\omega) = & -2\delta(r_2-r_1)\int r_3^2 dr_3 V^0(r_2,r_3)\int \frac{d\omega_1}{2\pi}\widetilde{G}(r_3,r_3,\omega_1) - 2\delta(r_2-r_1)\int r_3^2 dr_3 V^0(r_2,r_3)\int\int r_4^2 r_5^2 dr_4 dr_5 \\
& \times \int \frac{d\omega_1}{2\pi} i\Gamma_1(r_3,r_4,r_5,0,\omega_1)\widetilde{G}(r_5,r_4,\omega_1) + \int \frac{d\omega_1}{2\pi} G_0(r_2,r_1,\omega-\omega_1)\widetilde{V}(r_2,r_1,\omega_1) \\
& + \int \frac{d\omega_1}{2\pi}\int\int r_3^2 r_4^2 dr_3 dr_4 G_0(r_3,r_1,\omega-\omega_1) i\Gamma_1(r_4,r_3,r_2,\omega_1,\omega-\omega_1) V(r_4,r_1,\omega_1) \\
& + \int \frac{d\omega_1}{2\pi}\int\int r_3^2 r_4^2 dr_3 dr_4 \widetilde{V}(r_2,r_3,\omega_1) i\Gamma_1(r_3,r_1,r_4,-\omega_1,\omega) G_0(r_2,r_4,\omega-\omega_1)
\end{aligned}
\tag{20}
$$

where the first two terms are represented by S_1 in Fig. 9. The third term is represented by S_2 and the fourth and fifth terms by S_3. $\widetilde{G}$ is the dressed electron propagator with the zeroth-order propagator G_0 subtracted. $\widetilde{V}$ is, analogously, the dressed interaction V with the Coulomb interaction V^0 subtracted. In the first three terms these subtractions are done in order to avoid including any of the HF contributions. In the fifth term, contributing to S_3, $\widetilde{V}$ is used in order to avoid double counting the symmetric second-order term, as indicated in Fig. 9. $i\Gamma_1$ is the first-order vertex correction given by the first diagram in Fig. 11. The integrations over the energy ω_1 in all four terms is performed numerically, using a Wick rotation into the complex ω_1 plane.

(3) The Dyson equation (14) is set up using the self-energy operator $\Sigma^\star(r_2,r_1,\omega)$ evaluated in the previous step. The equation is solved, using matrix inversion, and the result is a dressed-electron propagator $G(r',r,\omega)$.

(4) The proper self-energy operator $\Sigma^\star(r_2,r_1,\varepsilon)$, which should be used in the QPE, is evaluated. The proper self-energy is evaluated here in the approximation indicated in Fig. 12, using the dressed electron propagators calculated in step (3) together with the screened interaction lines calculated in step (1).

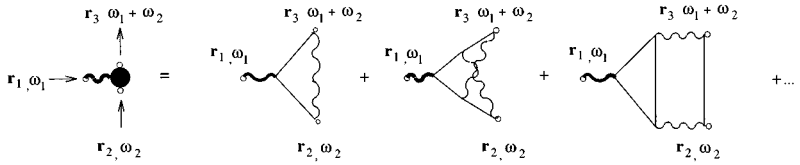

FIG. 10. Graphical representation of the vertex correction $\Gamma(r_1,r_2,r_3,\omega_1,\omega_2)$. Note that the incoming interaction line in r_1 is not included in the vertex correction, but is included in the figure for reasons of clarity.

(5) The self-energy operator $\Sigma^\star(r_2,r_1,\varepsilon)$ is added to $\hat{h}_0$, and the quasiparticle equation is solved in the same way as the zeroth-order equation. The resulting energy eigenvalue is the binding energy for the electron.

Since $\Sigma^\star$ is energy dependent, the process (1)–(5) should, in principle, be repeated until self-consistency is reached for the energy ε. The energy dependence of $\Sigma^\star$ is almost linear, and two iterations together with a linear extrapolation is usually enough, if a good first choice of the energy is made. For the alkali atoms treated in this paper the change in ε between iterations one and two is so small, less than 0.4% of the correlation energy, that even the second iteration can be omitted. This depends, of course, on the numerical accuracy that is wanted. In this paper, the second iteration was omitted after tests including the second- and third-order contributions to the proper self-energy $\Sigma^\star(\varepsilon)$.

B. Results and discussion

1. Second- and third-order self-energy calculations

In order to test the numerical accuracy of our procedure, we have evaluated the low-order contributions to the ground-state binding energy for the valence electron. The correction to the binding energy is first evaluated as the matrix element of the proper self-energy operator

$$W^\star = \langle \varphi_0 | \Sigma^\star(\varepsilon_0) | \varphi_0 \rangle, \tag{21}$$

where φ_0 is the zeroth-order orbital for the valence electron and ε_0 is the corresponding energy eigenvalue.

The electron propagators and the screened interaction lines were expanded in partial waves, each associated with a function of the radial coordinates. The radial coordinates were discretized with $r=e^x/Z$, where Z denotes the nuclear charge, and the grid points were equidistantly distributed in x from $x_{min}=-8.0$ to $x_{max}=6.0$, corresponding to the box size $R_{max}\approx 130$ a.u. for lithium, $R_{max}\approx 37$ a.u for sodium, and $R_{max}\approx 21$ a.u. for potassium. Two different grids with 41 and 61 points were used. The results from the two grids were extrapolated to account for the finite number of grid points used. The summations over angular momenta were truncated at l limits $l_{max}=2$, 3, 4 and 5. The results from the different l limits were then extrapolated in order to account for the complete angular-momentum sum. Energy integrals were evaluated using either calculus of residues or numerically, using Gaussian quadrature. In general, the proper polarization operator and the vertex correction were evaluated using calculus of residues and the proper self-energy operators, in Figs. 9 and 12, were evaluated numerically, using a Wick rotation of the integration contour into the complex ω plane and Gaussian quadrature techniques. For the self-energy operator used for dressing the electron propagator, 100 to 175 grid points in every integral were used. For the self-energy operator used in the QPE, only 60 grid points were needed. This yielded an accuracy of at least 1 part in 10^8 when compared with the results for the same effects evaluated using ordinary MBPT methods [8,15,43].

The second-order and third-order contributions to the proper self-energy, evaluated in this work, are given graphically in boxes I and II in Fig. 14. The results for all second- and third-order corrections to the valence electron binding energy are given in Tables I and II.

We have also solved the QPE, using the proper self-energy operator including the second- and third-order contributions. In this way, iterations of the proper self-energy operator are included to infinite order. The difference between the QPE eigenvalue and the HF eigenvalue then gives the total correlation energy due to the effects included in the proper self-energy operator. This method has, in recent years, been used in calculations of the valence-electron binding energies in negative alkaline-earth ions [38,39,44–47] and also in calculations of the cesium ground state [37].

The second-order corrections for the alkali metal atoms have also been evaluated by Johnson, Idrees, and Sapirstein [48]. Our results are in good agreement with the values obtained in Ref. [48].

For the alkali-metal atoms Li, Na, and K there are no previously published calculations of the third-order corrections to binding energy. A detailed analysis of the third-order corrections is, however, given for Cs and Tl by Blundell, Johnson, and Sapirstein in Ref. [40]. The third-order contributions to the proper self-energy operator, given in box II in Fig. 14, are interesting because a number of different types of conceptually important correlation effects enters into the perturbation expansion for the first time. Diagram F_1 in Fig. 14 represents an iteration of the polarization operator included in the second-order diagram G_1 in the same figure. Diagrams G_1 and F_1 are the leading corrections included in the random-phase approximation. Often, diagram F_1 is considered as direct process and the diagram F_2 as its exchange, and together with diagrams G_1 and G_2 they contribute to the *random-phase approximation with exchange* (RPAE) [32,33]. Diagrams F_{11}–F_{14} all contain electron propagators which are modified due to the electron correlation. These diagrams include the second-order electron propagators given in Fig. 4.

The results of our calculations of the third-order self-energy corrections to the energy are given in Table II. There

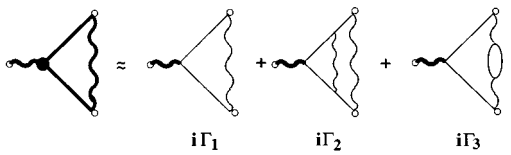

FIG. 11. The approximation of the vertex correction $\Gamma(r_1,r_2,r_3,\omega_1,\omega_2)$ used in this work.

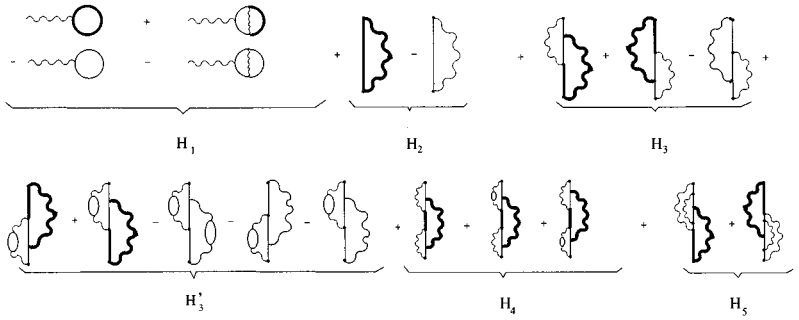

FIG. 12. Graphical expansion of the proper all-order self-energy operator used in this work when solving the quasiparticle equation. The thick lines denotes dressed electron propagators and screened interaction lines.

are several points to be made in connection with the third-order results. The first observation to make is that the dominating corrections for all three atoms in third order are diagrams F_1 and F_2. These diagrams are particularly large for potassium. The energy correction from F_1 is -51% of the total correlation energy for potassium and F_2 gives a 40% contribution to the correlation energy. Note also that there is a substantial cancellation between F_1 and F_2 for all three atoms.

For sodium and potassium the ladder diagrams F_8 and F_9 also give large individual contributions. These diagrams can, however, be expected to cancel each other to a large extent. This can be seen in the following way. Diagram F_8 can be interpreted as the interaction between the excited valence electron and the hole in the core, created when a core electron is virtually excited. Diagram F_9 can in the same way be interpreted as the interaction between the excited valence electron and the excited core electron. If the valence electron is far from the rest of the atom, it will see the combined field from the core hole and the electron excited out of the core. At large distances, this field will be zero and therefore diagrams F_8 and F_9 will cancel each other perfectly. Of course, the actual field from the electron and the core holes, seen by the valence electron, is not zero so the cancellation will be incomplete. For sodium the cancellation is very large. The remaining energy correction from F_8+F_9 in sodium is -0.9% of the total correlation energy. For potassium, on the other hand, the cancellation is much less pronounced. In this case F_8+F_9 give a -5.3% correction to the correlation energy. It can be argued that the same type of cancellation between the ladder diagrams will also occur in higher orders of perturbation theory and that the net contribution from the ladder diagrams will therefore be fairly small for these systems. If, however, the cancellation does not occur in higher orders, it is possible that the higher-order ladder diagrams will yield significant contributions.

The third point to be noted is the large contribution from diagrams F_3 and F_4 for sodium. The diagrams represent a polarization modification of the second-order exchange diagram G_2. For both lithium and potassium the contribution from F_3+F_4 is much smaller than the contribution from G_2. For sodium, on the other hand, F_3+F_4 is almost three times larger than G_2. Also, for diagrams F_{11}–F_{14}, sodium and potassium behave differently from each other. In the sodium case, both F_{11} and F_{13} give large contributions to correlation energy, while for potassium F_{11} is negligible.

2. Fourth-order self-energy corrections

In our approach, a large fraction of the fourth-order contributions to the proper self-energy are included. As pointed out before, we found 122 contributing Feynman diagrams, Hermitian conjugates included, in fourth order if HF was used as the zeroth-order model. In our approach, 34 of these diagrams are included and we have also evaluated them explicitly here. All evaluated fourth-order diagrams are given in box III in Fig. 14 and the numerical results are given in Table III.

When analyzing the fourth-order results, it is more adequate to investigate the contributions from the groups of diagrams originating from the different skeletons in Fig. 7 than the results for the individual diagrams. There are substantial cancellations within the groups and the total contributions from several of the groups are significantly smaller than the individual diagrams.

The first group of fourth-order diagrams in Fig. 14, $F_{15}-F_{26}$, contribute to part H_2 of the proper self-energy operator in Fig. 12. This part of the self-energy operator originates from skeleton 2 in Fig. 7. All correlation modifications of the skeleton are either self-energy insertions on the electron line or polarization insertions on the interaction line. Diagrams $F_{15}-F_{26}$ are divided into three subgroups. $F_{15}-F_{18}$ contain higher-order modifications of the interaction line, while the electron propagator is given by the zeroth-order approximation G_0. Diagrams $F_{19}-F_{24}$ contain third-order self-energy modifications of the electron propagator but no modification of the interaction line. Finally, diagrams F_{25} and F_{26} contain both second-order self-energy insertions on the electron line and screening of the interaction line.

The first subgroup, $F_{15}-F_{18}$, is of particular interest, since, in general, these diagrams give the largest individual contributions but also the largest cancellations between the diagrams. For lithium, the largest evaluated fourth-order diagram is F_{18}, which gives a 5.6% contribution to the correlation energy. The total contribution from the subgroup is, however, only 1.8% of the total correlation energy. The situ-

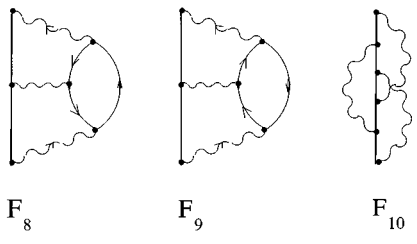

FIG. 13. Third-order diagrams added to the proper self-energy operator in order to make it complete to third order in perturbation theory.

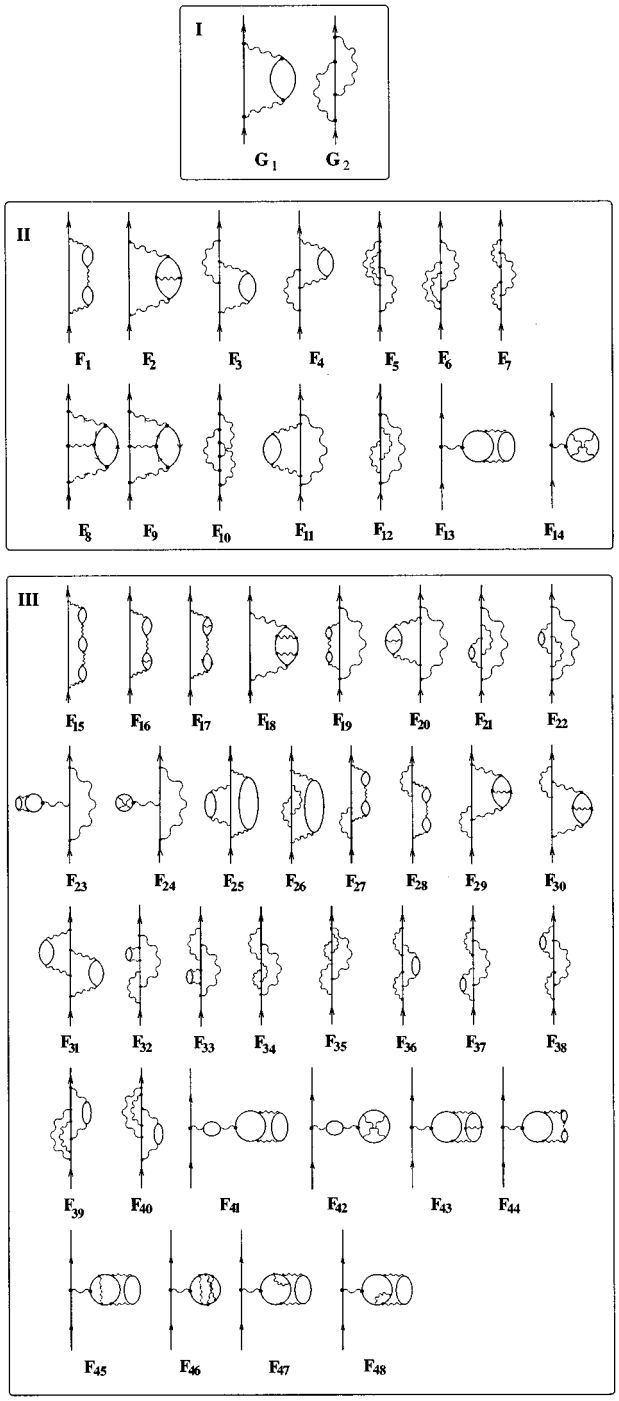

FIG. 14. Second-, third-, and fourth-order contributions to the ground-state energy, evaluated for lithium, sodium, and potassium in this paper.

ation is similar for sodium. F_{18} gives a 4.8% contribution while the total contribution from the subgroup is only 1.3%. For potassium, the cancellations within this subgroup are very large. F_{15} gives a 34.4% contribution to the correlation energy, $F_{16}+F_{17}$ gives -44.8%, and F_{18} gives 16.3%. The total contribution from the subgroup to the correlation energy is, however, only 5.9%. This demonstrates the importance of a systematic inclusion of the low-order diagrams in the proper self-energy operator. If, for example, the proper polarization is approximated with only skeleton 1 in Fig. 8,

TABLE I. Second-order self-energy contributions to the correlation energy in millihartrees for Li $2s$, Na $3s$, and K $4s$. G_1 and G_2 refer to the second-order diagrams given in box I in Fig. 14. The relativistic correction is defined as the difference between the Dirac-Fock and the Hartree-Fock energies.

Diagram	Li $2s$	Na $3s$	K $4s$
G_1	-2.094	-6.099	-13.448
G_2	0.445	0.247	1.142
Sum:	-1.649	-5.852	-12.305
QPE:	-197.967	-187.900	-160.551
Correlation:	-1.663	-6.099	-13.597
Relativity:	-0.016	-0.232	-0.536
QPE+relativity:	-197.983	-188.132	-161.087
Experiment:	-198.159	-188.859	-159.517
Hartree-Fock:	-196.304	-181.801	-146.954

diagrams F_1 in third order and F_{15} in fourth order are included, while diagram F_2 in third order and diagrams $F_{16}-F_{18}$ in fourth order are omitted and the important cancellation does not occur.

The second subgroup, contributing to H_2 in Fig. 12, is given by diagrams $F_{19}-F_{24}$. For both lithium and potas-

TABLE II. Third-order self-energy contributions to the correlation energy, in millihartree, for Li $2s$, Na $3s$, and K $4s$. F_n refers to the third-order diagrams given in box II in Fig. 14. The relativistic correction is defined as the difference between the Dirac-Fock and the Hartree-Fock energies.

Diagram	Li $2s$	Na $3s$	K $4s$
2nd order	-1.649	-5.852	-12.305
QPE (2nd)	-197.967	-187.900	-160.551
F_1	0.177	0.993	6.151
F_2	-0.398	-1.303	-4.764
F_3	0.061	0.337	-0.102
F_4	0.061	0.337	-0.102
F_5	0.016	-0.115	0.237
F_6	0.016	-0.115	0.237
F_7	-0.075	-0.178	-0.035
F_8	-0.048	-0.446	-2.722
F_9	0.054	0.505	3.352
F_{10}	0.044	0.122	-0.421
F_{11}	-0.060	-0.356	0.014
F_{12}	0.030	0.094	-0.019
F_{13}	0.003	-0.287	0.555
F_{14}	-0.001	0.079	-0.161
Sum:	-0.120	-0.333	2.220
Sum (2nd +3rd order):	-1.769	-6.185	-10.085
QPE:	-198.089	-188.249	-157.791
Correlation:	-1.785	-6.448	-10.836
QPE+Relativity:	-198.105	-188.481	-158.327

TABLE III. The fourth-order self-energy energy contributions to the correlation energy in millihartrees, evaluated in this work, for Li $2s$, Na $3s$, and K $4s$. F_n refers to the fourth-order diagrams given in box III in Fig. 14. The relativistic correction is defined as the difference between the Dirac-Fock and the Hartree-Fock energies.

Diagram	Li $2s$	Na $3s$	K $4s$
2nd+3rd order	-1.769	-6.185	-10.085
QPE (2nd+3rd)	-198.089	-188.249	-157.791
F_{15}	-0.022	-0.252	-4.139
F_{16}	0.046	0.247	2.689
F_{17}	0.046	0.247	2.689
F_{18}	-0.102	-0.329	-1.964
F_{19}	0.009	0.355	0.071
F_{20}	-0.008	-0.192	-0.070
F_{21}	-0.009	-0.114	-0.006
F_{22}	-0.009	-0.114	-0.006
F_{23}	0.002	0.017	-0.027
F_{24}	-0.001	-0.003	0.018
F_{25}	-0.016	-0.036	-0.181
F_{26}	0.007	0.010	0.035
F_{27}	-0.026	-0.252	0.090
F_{28}	-0.026	-0.252	0.090
F_{29}	0.034	0.149	-0.049
F_{30}	0.034	0.149	-0.049
F_{31}	-0.001	-0.076	-0.147
F_{32}	0.008	0.010	0.103
F_{33}	0.008	0.010	0.103
F_{34}	-0.003	-0.007	-0.035
F_{35}	-0.003	-0.007	-0.035
F_{36}	0.034	0.148	0.095
F_{37}	0.006	0.029	-0.028
F_{38}	0.006	0.029	-0.028
F_{39}	0.019	0.122	-0.055
F_{40}	0.019	0.122	-0.055
F_{41}	-0.003	0.082	-0.357
F_{42}	0.002	-0.029	0.098
F_{43}	-0.032	-0.275	-0.022
F_{44}	0.020	0.463	-0.072
F_{45}	-0.001	-0.097	0.171
F_{46}	0.000	0.028	-0.050
F_{47}	-0.012	-0.146	0.065
F_{48}	-0.012	-0.146	0.065
Sum:	0.010	-0.112	-0.991
Sum (2nd+3rd+4th):	-1.760	-6.297	-11.078
QPE:	-198.077	-188.349	-159.024
Correlation:	-1.773	-6.548	-12.070
QPE+Relativity:	-198.093	-188.581	-159.560

sium, all diagrams in this subgroup are smaller than 1% of the correlation energy. The total contribution from this subgroup is 0.9% for lithium and 0.4% for potassium. For sodium the situation is somewhat different. Diagrams $F_{19}-F_{22}$ are, in this case, fairly large. F_{19} is -5.2% of the correlation energy, F_{20} is 2.8% and $F_{21}+F_{22}$ gives a 3.4% contribution. Still, the total contribution from the subgroup is only 0.7%.

The next group of fourth-order diagrams, F_{27}–F_{35} in Fig. 14, contributes to part H_3+H_3' of the self-energy operator in Fig. 12. These diagrams originate from skeleton 3 in Fig. 7. For lithium and sodium, the group is dominated by diagrams $F_{27}+F_{28}$ and $F_{29}+F_{30}$. In lithium, $F_{27}+F_{28}$ contributes with 2.8% and in sodium with 7.4%. $F_{29}+F_{30}$, on the other hand, gives -3.6% for lithium and -4.4% for sodium. The total contribution to the correlation energy from this group is -1.3% for lithium and 4.0% for sodium. In the potassium case, all diagrams in the group except F_{31} are smaller than 1% in size. The total contribution from this group for potassium is only -0.6%.

Diagrams $F_{36}-F_{40}$ contribute to parts H_4 and H_5 of the self-energy operator in Fig. 12. For both lithium and sodium, these diagrams yield large contributions. In lithium, the total contribution from these diagrams is -4.4% and in sodium it is -6.6% of the correlation. For potassium the contribution is only 0.6%.

The final group of fourth-order diagrams, $F_{41}-F_{48}$, contributes to part H_1 of the self-energy operator in Fig. 12. For lithium and sodium, the group is dominated by the diagrams F_{43}, F_{44}, and $F_{47}+F_{48}$. For lithium, the largest diagram in the group is F_{43}, which gives a 1.7% contribution. $F_{47}+F_{48}$ contribute 1.4% to the correlation energy and F_{44} -1.1%. The total contribution from the group for lithium is 2.1%. For sodium all diagrams in the group except F_{42} and F_{46} are larger in size than 1% of the correlation energy. Large contributions come from F_{43} and $F_{47}+F_{48}$, which together are as large as 8.2%. This is cancelled to a large extent by F_{44} which is -6.8%. The total contribution from the group for sodium is only 1.8%. Finally, for potassium only F_{41} and F_{45} are larger than 1% in size. The total contribution from this group for potassium is 0.9%.

The contribution from all evaluated fourth-order diagrams is -0.6% of the correlation energy for lithium, 1.6% for sodium, and 8.2% for potassium. Thus, the proper self-energy including all second- and third-order effects and the class of fourth-order effects evaluated in this paper accounts in lithium for 95.7% of the correlation energy, in sodium for 92.2%, and in potassium for 92.1%. The total correlation energy accounted for with this approximation of the proper self-energy operator is deduced as the difference between the QPE eigenvalue and the HF eigenvalue. For lithium, the result is -1.773 mhartree, which corresponds to 96.4% of the correlation energy. For sodium, the result is -6.548 mhartree, which is equal to -95.9% of the correlation energy. Finally, for potassium the calculated correlation energy is -12.070 mhartree, which is 100.4% of the correlation.

It is clear from the low-order calculations, presented in this paper, that a large portion of the low-order effects make significant contributions to the correlation energy. In third order almost all diagrams are larger in size than 1% of the correlation and we have also in fourth-order identified sev-

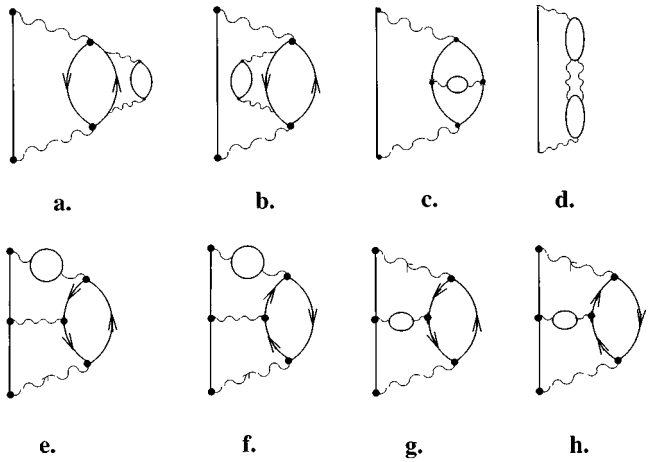

FIG. 15. Fourth-order self energies likely to give large contributions to the proper self-energy operator.

eral important effects. We have also found that there are large cancellations between the leading effects. Thus, for these atoms there seems to be no substitute for the most complete possible calculation, with respect to the low orders of perturbation theory. It must be emphasized that calculation of the effects $F_{15}-F_{48}$, presented in this paper in no sense represents a complete calculation of fourth order. In Fig. 15 a set of fourth-order Feynman diagrams, not included in the calculations, are given, which we consider likely to make significant contributions to the proper self-energy operator.

It is also clear that higher orders in perturbation theory play a crucial role in accurate calculations of the binding energy in these atoms. We now turn to this subject and discuss the results from our all-order calculations.

3. All-order self-energy calculations

In the final calculations we evaluated the proper self-energy operator in the approximation given in Fig. 12. The dressed electron propagators and interaction lines were evaluated, as previously discussed, by solving the Dyson equations (14) and (19). The contributions to the proper self-energy, $W^{\star}$ in Eq. (21), from the dressed skeletons, H_1-H_5 in Fig. 12, were evaluated also in this case. The quasiparticle equation was solved, using this dressed proper self-energy operator. The results from these calculations are given in Table IV.

The first observation to make is that the proper self-energy is dominated by H_2. H_2 gives for lithium 134% of the correlation energy, for sodium 99.7%, and for potassium 103%. The large size of H_2 is mainly due to the fact that the second-order diagram G_1 is included here, but also higher-order core polarization effects such as F_1, F_2, F_{15}, $F_{16}+F_{17}$ and F_{18}, in Fig. 14, are included.

For lithium, the large overestimation of the correlation by H_2 is compensated by H_3+H_3', which gives a -32.7% contribution. The contribution from H_1 is only 0.9%, H_4 contributes with 1.5% and H_5 with -4.4%. In lithium, this proper self-energy accounts for 96.0% of the correlation. The total correlation energy due to the effects $H_1+H_2+H_3+H_3'+H_4+H_5$, included in the proper self-energy operator, is again deduced as the difference between the QPE eigenvalue and HF eigenvalue. For lithium, our result is -1.780 millihartree (mhartree), which corresponds to 96.8% of the total correlation energy in lithium.

TABLE IV. Final results. Contributions to the correlation energy, in millihartrees, calculated using dressed electron propagators and screened interaction lines, for Li $2s$, Na $3s$ and K $4s$. The notation H_n refers to Fig. 12. The remaining third-order contributions added is the sum $F_8+F_9+F_{10}$. The relativistic correction is defined as the difference between the Dirac-Fock and the Hartree-Fock energies.

Diagram	Li $2s$	Na $3s$	K $4s$
H_1	-0.016	-0.340	0.244
H_2	-2.456	-6.807	-12.383
H_3+H_3'	0.602	0.705	0.898
H_4	-0.027	-0.029	-0.016
H_5	0.081	-0.045	0.430
Remaining 3rd order	0.051	0.180	0.208
Sum:	-1.766	-6.333	-10.619
QPE:	-198.084	-188.408	-158.453
Correlation:	-1.780	-6.607	-11.499
QPE+Relativity:	-198.100	-188.640	-158.989

For sodium and potassium, H_1 and H_3+H_3' are comparable in size. H_1 contributes with 5.0% and H_3+H_3' with -10.3%. In potassium, H_1 contributes with -2.0% and H_3+H_3' with -7.5%. Furthermore, H_4+H_5 gives a 1.1% contribution in sodium and a -3.5% contribution in potassium. The evaluated proper self-energy for sodium accounts for 92.8% of the correlation energy and for potassium we get 88.3%. In addition, we have the effects coming from iterations of the proper self-energy. As mentioned, these are taken into account by solving the quasiparticle equation leading to the total result -6.607 mhartree, corresponding to 96.8% of the correlation energy in sodium. For potassium our total result is -11.499 mhartree, which is 95.6% of the correlation energy.

Finally, in Table V a comparison with some accurate CCSD calculations is presented. For both lithium and potassium, the CCSD results [14,16,43,40] agree very well with the experimental results. For sodium, on the other hand, the agreement with experiment is relatively poor. In this case, the CCSD method only manages to account for 94% of the correlation energy. Blundell, Johnson, and Sapirstein [49] and Salomonson and Ynnerman [43,16] also evaluated the the so-called $E^{(3)}_{extra}$ terms, which can be considered as a Hermitian-conjugate correction to CCSD. For both lithium and sodium, the $E^{(3)}_{extra}$ correction was found to be very small. For lithium it was found to be 0.011 mhartree [49] and for sodium -0.030 mhartree [43]. However, for potassium the correction was found to be huge. In this case the $E^{(3)}_{extra}$ contributes with 1.396 mhartree [16], which completely spoils the agreement with experiment for potassium. Salomonson and Ynnerman also evaluated, for sodium and potassium, a class of three-particle effects which are expected to be important. When including these effects, very good agreement with experiment for sodium was found but

TABLE V. Comparison with other calculations. Energies are given in millihartrees.

		Li 2*s*	Na 3*s*	K 4*s*
This work	Correlation	-1.780	-6.607	-11.499
	Binding energy	-198.100	-188.640	-158.989
This work+three-particle effects in Refs. [43,16]	Correlation		-6.852	-11.880
	Binding energy		-188.852	-159.369
CCSD	Correlation	-1.834[a]	-6.428[c]	-12.044[d]
	Binding energy	-198.154[a]	-188.461[c]	-159.534[d]
Relative CCSD+$E^{(3)}_{extra}$	Correlation	-1.841[b]		
	Binding energy	-198.142[b]		
CCSD+$E^{(3)}_{extra}$+rel +three-particle effects	Correlation		-6.840[c]	-11.250[d]
	Binding energy		-188.873[c]	-158.740[d]
Experiment		-198.159	-188.859	-159.517

[a]I. Lindgren [14].
[b]Blundell *et al.* [49].
[c]S. Salomonson and A. Ynnerman [43].
[d]A. Ynnerman [16].

only 93.5% of the correlation was accounted for in potassium.

A large subset of the three-particle effects, evaluated by Salomonson and Ynnerman, are not included in the approximations used in this paper. Certain time orders of the diagrams *a*, *b*, *c*, *g*, and *h* in Fig. 15 and higher-order diagrams of these types were included in their calculation. For sodium these effects were found to contribute with -0.245 mhartree and for potassium -0.381 mhartree. If these effects are added to the correlation energy evaluated in this work (see Table V), we get -6.852 mhartree for sodium and -11.879 mhartree for potassium. This corresponds to 100.4% of the correlation for sodium and 98.8% for potassium.

IV. CONCLUSIONS

In this paper we have applied an alternative approach to the atomic MBPT, the single-particle Green's-function method, based on time-dependent perturbation theory and the diagrammatic formulation of quantum field theory. We have presented an all-order evaluation scheme for the proper self-energy operator which is based on the systematic use of Dyson's integral equations for both the electron propagator and the screened Coulomb interaction. The evaluated self-energy operator is complete to third-order in perturbation theory and also includes a large amount of higher-order effects. The proper self-energy operator contains important classes of many-body effects beyond the pair-correlation approximation.

In order to test our method, we have carried out extensive calculations on the ground-state valence-electron binding energy for the alkali-metal atoms Li, Na, and K. We have investigated the low-order behavior of the perturbation expansion for these systems in order to identify important classes of contributions to the proper self-energy operator. We have also carried out all-order calculations of the valence-electron binding energy using the proposed evaluation method. The results are found to be in good agreement with experiment. The numerical results for the correlation energy for the different atoms are consistent with each other. Approximately 96–97 % of the correlation energy is accounted for in all three atoms in this approach. This is in contrast to the results for the same binding energies obtained with the CCSD method, which are somewhat mutually contradictory, as shown by Salomonson and Ynnerman [43,16].

It is reasonable to assume that the remaining correlation energy can, to a large extent, be explained by higher-order polarization effects and ladder effects, which were neglected in this work. This conclusion can be drawn when one takes into account that we get 100% of the correlation energy for sodium and 99% for potassium if the contributions from the classes of three-particle effects, evaluated by Salomonson and Ynnerman, are added to our results.

ACKNOWLEDGMENTS

We would like to thank Dr. A.-M. Pendrill, Dr. H. Persson, and P. Sunnergren for many helpful discussions. The work has been supported by the Swedish Natural Science Research Council and the Knut och Alice Wallenberg Foundation.

[1] K. Brueckner, Phys. Rev. **100**, 36 (1955).
[2] J. Goldstone, Proc. R. Soc. London Ser. A **239**, 267 (1957).
[3] H. P. Kelly, Phys. Rev **131**, 684 (1963).
[4] H. Kelly, Adv. Chem. Phys. **14**, 129 (1969).
[5] B. Brandow, Rev. Mod. Phys. **39**, 771 (1967).
[6] P. Sandars, Adv. Chem. Phys. **14**, 365 (1969).
[7] I. Lindgren, J. Phys. B **7**, 2441 (1974).
[8] I. Lindgren and J. Morrison, *Atomic Many-Body Theory*, 2nd ed. (Springer-Verlag, Berlin, 1985).
[9] F. Coester, Nucl. Phys. **7**, 421 (1958).
[10] F. Coester and H. Kümmel, Nucl. Phys. **17**, 477 (1960).
[11] J. Čížek, J. Chem. Phys. **45**, 4256 (1966).
[12] J. Čížek, Adv. Chem. Phys. **14**, 35 (1969).
[13] G. Purvis and J. Bartlett, J. Chem. Phys. **76**, 1910 (1995).
[14] I. Lindgren, Phys. Rev. A **31**, 1273 (1985).
[15] S. Salomonson and P. Öster, Phys. Rev. A **41**, 4670 (1990).
[16] A. Ynnerman, Ph.D. thesis, Göteborg University, Chalmers University of Technology, Göteborg, 1992.
[17] R. Feynman, Phys. Rev. **76**, 749 (1949).
[18] R. Feynman, Phys. Rev. **76**, 769 (1949).
[19] M. Gell-Mann and F. Low, Phys. Rev. **84**, 350 (1951).
[20] F. Dyson, Phys. Rev. **75**, 486 (1949).
[21] F. Dyson, Phys. Rev. **75**, 1736 (1949).
[22] A. Fetter and J. Walecka, *Quantum Theory of Many-Particle Systems*, 1st ed. (McGraw-Hill, New York, 1971).
[23] R. Mattuck, *A Guide to Feynman Diagrams in the Many-Body Problem* (Dover, New York, 1976).
[24] I. Lindgren, J. Phys. B **24**, 1143 (1991).
[25] J. Lindeberg and Y. Öhrn, *Propagators in Quantum Chemistry* (Academic, London, 1973).
[26] Y. Öhrn, *The World of Quantum Chemistry*, edited by B. Pullman and R. Parr (Reidel, Dordrecht, 1976), p. 57.
[27] L. Cederbaum and W. Domcke, Adv. Chem. Phys. **36**, 205 (1977).
[28] W. von Niessen, J. Schirmer, and L. Cederbaum, Comp. Phys. Rep. **1**, 58 (1984).
[29] J. Oddershede, Adv. Chem. Phys. **59**, 201 (1987).
[30] O. Walter and J. Schirmer, J. Phys. B **14**, 3805 (1981).
[31] J. Schirmer, L. S. Cederbaum, and O. Walter, Phys. Rev. A **28**, 1237 (1983).
[32] M. Amusia and N. Cherepkov, Case Studies in Atomic Physics **5**, 47 (1975).
[33] G. Wendin, in *Photoionization and Other Probes of Many-Electron Interactions*, edited by F. Wuilleumier, *NATO Advanced Study Institute Series B: Physics* (Plenum, New York, 1976), pp. 61–84.
[34] G. Wendin and M. Ohno, Phys. Scr. **14**, 148 (1976).
[35] G. Wendin, Structure and Bonding **45**, (1981).
[36] V. Dzuba, F. Flambaum, P. Silvestrov, and O. Sushkov, Phys. Lett. A **131**, 461 (1988).
[37] V. Dzuba, F. Flambaum, and O. Sushkov, Phys. Lett. A **140**, 493 (1989).
[38] V. Dzuba, F. Flambaum, F. Gribakin, and D. Sushkov, Phys. Rev. A **44**, 2823 (1991).
[39] V. Dzuba and F. Gribakin, Phys. Rev. A **49**, 2483 (1994).
[40] S. Blundell, W. Johnson, and J. Sapirstein, Phys. Rev. A **42**, 3751 (1990).
[41] G. Wick, Phys. Rev. **80**, 268 (1950).
[42] S. Salomonson and P. Öster, Phys. Rev. A **40**, 5559 (1989).
[43] S. Salomonson and A. Ynnerman, Phys. Rev. A **43**, 88 (1991).
[44] L. Chernysheva, F. Gribakin, V. Ivanov, and M. Kuchiev, J. Phys. B **21**, L419 (1988).
[45] W. Johnson, J. Sapirstein, and S. Blundell, J. Phys. B **22**, 2341 (1989).
[46] F. Gribakin, B. Gultsev, V. Ivanov, and M. Kuchiev, J. Phys. B **23**, 4505 (1990).
[47] S. Salomonson, H. Warston, and I. Lindgren, Phys. Rev. Lett. **76**, 3092 (1996).
[48] W. Johnson, M. Idrees, and J. Sapirstein, Phys. Rev. A **35**, 3218 (1987).
[49] S. Blundell, W. Johnson, and J. Sapirstein, Phys. Rev. A **40**, 2233 (1989).